RESEARCH ARTICLE

Macromolecular Bioscience
www.mbs-journal.de

Toward Highly Matching the Dura Mater: A Polyurethane Integrating Biocompatible, Leak-Proof, and Self-Healing Properties

Pandi Chen, Fenglong Li, Guyue Wang, Binbin Ying, Chao Chen, Ying Tian, Maosong Chen, Kyung Jin Lee, Wu Bin Ying, and Jin Zhu**

The dura mater is the final barrier against cerebrospinal fluid leakage and plays a crucial role in protecting and supporting the brain and spinal cord. Head trauma, tumor resection and other traumas damage it, requiring artificial dura mater for repair. However, surgical tears are often unavoidable. To address these issues, the ideal artificial dura mater should have biocompatibility, anti-leakage, and self-healing properties. Herein, this work has used biocompatible polycaprolactone diol as the soft segment and introduced dynamic disulfide bonds into the hard segment, achieving a multifunctional polyurethane (LSPU-2), which integrated the above mentioned properties required in surgery. In particular, LSPU-2 matches the mechanical properties of the dura mater and the biocompatibility tests with neuronal cells demonstrate extremely low cytotoxicity and do not cause any negative skin lesions. In addition, the anti-leakage properties of the LSPU-2 are confirmed by the water permeability tester and the 900 mm H_2O static pressure test with artificial cerebrospinal fluid. Due to the disulfide bond exchange and molecular chain mobility, LSPU-2 could be completely self-healed within 115 min at human body temperature. Thus, LSPU-2 comprises one of the most promising potential artificial dura materials, which is essential for the advancement of artificial dura mater and brain surgery.

1. Introduction

The dura mater, a membrane located beneath the skull that covers the brain and spinal cord, is composed of scattered fibroblasts, coiled collagen fibers, and elastin fibers.[1] Due to its excellent elasticity and toughness, this membrane can protect and support the delicate tissues beneath, as well as prevent cerebrospinal fluid leakage.[2] However, head trauma, tumor resection, and other traumas damage it, requiring artificial dura mater for repair. More importantly, clinical emergencies involving the brain (e.g., acute subdural hematoma, severe cerebral contusion, and acute cerebral hemorrhage) can also tear or damage the dura mater, resulting in immediate herniation of the brain.[3] In clinical settings, a craniotomy is commonly performed for the removal of a life-threatening hematoma and decompressive craniectomy.[4] During the surgical procedure, the dura mater is sectioned and then repaired with an artificial dura membrane in order to reduce intracranial pressure.[5] Following recovery, patients should have their skulls repaired. The success rate of skull repair, on the other hand, depends heavily on the properties of the artificial dura mater. This is due to the fact that tearing of the artificial dura mater during skull repair surgery can result in a number of complications that affect the prognosis.[6]

With the development of biomaterials and tissue engineering technology, novel materials for restoring the anatomical integrity

P. Chen, M. Chen
Department of Neurosurgery
the Affiliated Lihuili Hospital of Ningbo University
Ningbo 315040, P. R. China

F. Li, G. Wang, C. Chen, Y. Tian, W. B. Ying, J. Zhu
Key Laboratory of Bio-based Polymeric Materials Technology and Application of Zhejiang Province
Ningbo Institute of Materials Technology and Engineering
Chinese Academy of Sciences
Ningbo 315201, P. R. China
E-mail: yingwubin@nimte.ac.cn; jzhu@nimte.ac.cn

The ORCID identification number(s) for the author(s) of this article can be found under https://doi.org/10.1002/mabi.202300111

DOI: 10.1002/mabi.202300111

F. Li, C. Chen, Y. Tian
University of Chinese Academy of Sciences
Beijing 100049, P. R. China

G. Wang
Beijing Advanced Innovation Center for Materials Genome Engineering
School of Materials Science and Engineering
University of Science and Technology Beijing
Beijing 100083, P. R. China

B. Ying
Department of Mechanical Engineering
Massachusetts Institute of Technology
Cambridge, MA 02139–4307, USA

K. J. Lee
Department of Chemical Engineering and Applied Chemistry
Chungnam National University
Yoo-Seong 34134, Republic of Korea

of the dura mater and reducing postoperative complications have garnered the interest of surgeons and researchers.[7] Accordingly, numerous substances have been used as artificial dura mater.[8] Due to the limitations of comprehensive performance and complications, however, materials that can fully meet the requirements for clinical use have been largely limited. For instance, the autologous tissue-derived dural substitute has the benefits of no immune rejection, low incidence of postoperative complications, and low infection risk.[9] However, the size and shape of autologous dural substitutes are extremely limited, and they cannot be used to repair large dural defects. People also use synthetic materials such as polycaprolactone (PCL) or poly-L-lactic acid (PLLA) as dural repair materials.[8c,10] These materials performed well in biocompatibility, inflammatory response, and prevention of cerebrospinal fluid leakage, but their mechanical properties were difficult to match those of the dura mater, which may be the greatest challenge during practical application.[11]

Cranioplasty after craniotomy is one of the most common and fundamental neurosurgical procedures.[12] During surgery, surgeons typically make an incision along the defect of the skull, then cut the scalp down to the temporalis fascia and lift the scalp, before cutting and releasing a portion of the temporalis. Notably, the temporalis fascia and temporalis are frequently firmly attached to the previously repaired artificial dura mater in clinical practice. However, even when the operation is performed meticulously, dural breakage may still occur, even with multiple breakages during a single operation. Once a dural tear has occurred, it is necessary to fill the tear with a gelatin sponge and repair the artificial meninges using silk sutures. This operation will be not only time-consuming but also greatly increase the probability of postoperative cerebrospinal fluid leakage and scalp hydrops significantly. If the dura mater is not closely repaired, long-term postoperative scalp hydrops may develop, leading to poor wound healing, an elevated risk of incision infection or intracranial infection, and even reoperation.[6] If the artificial dura mater has the ability to self-heal, the complications listed above, such as artificial dural rupture, cerebrospinal fluid leakage, and scalp hydrops, could be effectively avoided.[13] Self-healing elastomers have the potential to become important materials for artificial dura mater due to their flexible mechanical properties. Based on the different healing mechanisms, self-healing elastomers can be divided into externally driven and internally driven types.[14] Externally driven self-healing involves releasing pre-embedded external healing agents in the damaged area of the elastomer to achieve self-repair.[15] This method is simple, convenient and does not require complex molecular design to achieve self-healing. However, its disadvantage is also obvious: it cannot achieve long-term and repeated spontaneous repair of the damaged elastomer. This self-healing method has gradually been replaced by internally driven self-healing. Internally driven healing involves introducing self-healing driving forces through molecular design, without the need for external healing agents, allowing the molecular chains of the elastomer to spontaneously move and re-entangle, resulting in repeated self-healing. Internally driven healing is usually divided into reversible covalent bonds (such as disulfide bonds, Diels-Alder reactions, and boronic ester bonds) and dynamic non-covalent interactions (such as hydrogen bonds, ion bonds, metal coordination bonds, and host-guest structures).[16] The application of internally driven self-healing elastomers in artificial dura mater can lead to a significant alleviation of patients' suffering from related complications, as well as a drastic reduction in hospitalization duration and costs.

In conclusion, the ideal dural substitute should meet the following criteria: 1) Elasticity & toughness, which can withstand suture force and automatically wrap on damaged tissue;[17] 2) Good biocompatibility, which has no immune response;[18] 3) Excellent compactness, which can prevent cerebrospinal fluid leakage;[19] 4) Rapid self-healing capacity, which can prevent serious medical accidents caused by unanticipated damage.[20] As an artificial dura material that meets the aforementioned criteria, polyurethane is a good option.[21] Polyurethane is a block polymer with both hard and soft segments.[22] By adjusting the ratio of the hard segment to the soft segment, not only is it possible to obtain the desired mechanical properties but also the crystallinity and compactness of polyurethane can be controlled.[23] Moreover, the diversity of polyurethane structure can endow it with various functionalities, including biocompatibility, anti-leakage, self-healing, etc.[24]

Herein, we have designed a series of multifunctional polyurethanes for artificial dura mater with biocompatibility, anti-leakage, and self-healing properties. In particular, PCL diol was used as the soft segment, whereas a chain extender with dynamic disulfide bonds and isophorone diisocyanate was used as the hard segment. The ratio of hard-to-soft segments was adjusted appropriately to achieve the optimal mechanical properties that match the dura mater and its anti-leakage performance. Due to its non-toxic constituents, this polyurethane possesses excellent biocompatibility. Furthermore, within the ambit of the discussed self-healing driving forces, disulfide bonds have emerged as an exceedingly promising choice for our research owing to their lower bond energy and ability to undergo facile bond exchange at ambient temperature.[25] The aromatic disulfide bonds were introduced into the hard segments to endow polyurethane with good self-healing capacity with the aid of the excellent molecular chain mobility provided by the soft segment.[26] Thus, a biocompatible, leak-proof, and self-healing polyurethane with the potential to become one of the ideal artificial dura materials could be created.

2. Results and Discussion

Scheme 1 illustrates the various properties necessary for an artificial dura mater during brain surgery, including elasticity, toughness, biocompatibility, anti-leakage, and self-healing properties. The dura mater may be torn or damaged by head trauma, tumor resection, spinal cord surgery, etc., necessitating repair with an artificial dura mater. In addition to basic properties such as mechanical properties, biocompatibility, and anti-leakage, artificial dura mater must also possess the ability to heal itself. This is because the temporalis muscle fascia and temporalis muscle are tightly connected to the repaired artificial dura mater during cranioplasty. Thus, even with a careful operation, the artificial dura mater is likely to be compromised. Self-healing capacity could reduce postoperative complications like cerebrospinal fluid leakage and scalp hydrops. Therefore, the objective of this study is to develop an artificial dura mater with integrated

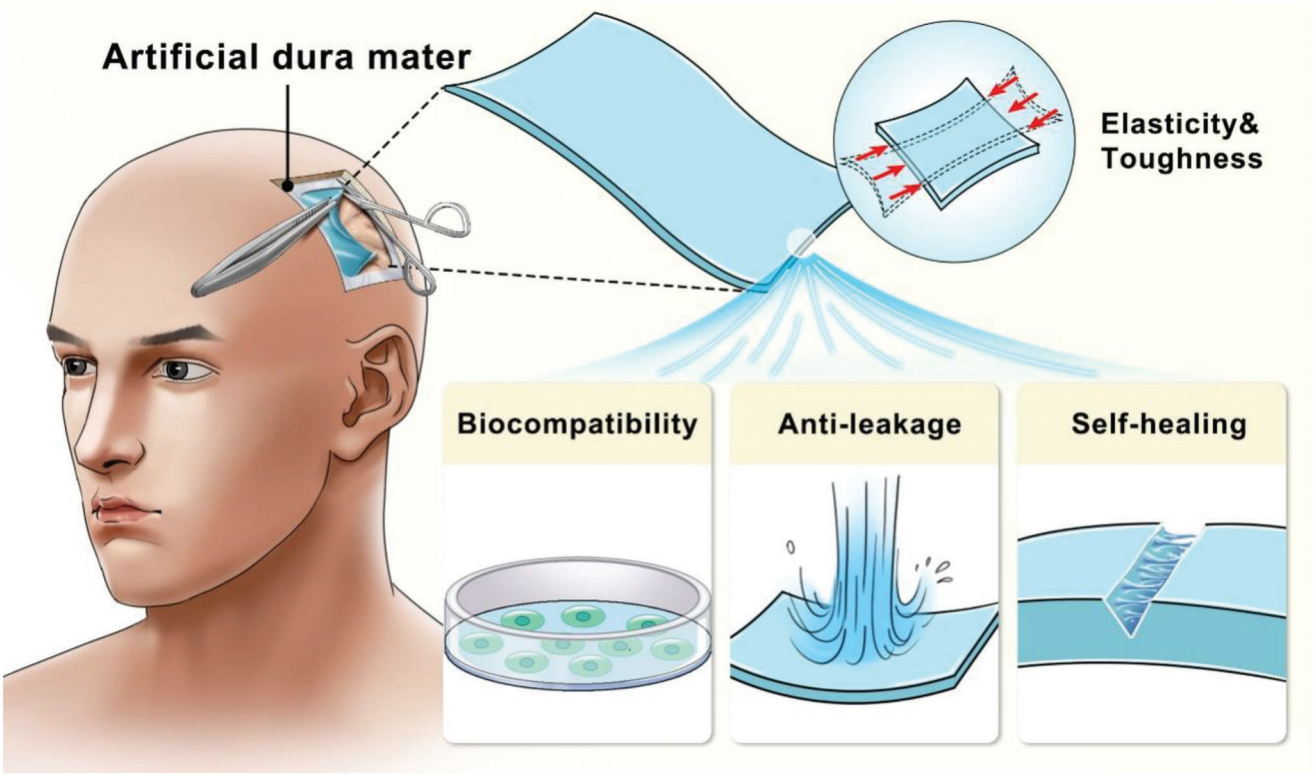

Scheme 1. Schematic illustration of the ideal artificial dura mater with elastic, tough, biocompatible, anti-leakage, and self-healing properties.

elasticity, toughness, biocompatibility, anti-leakage, and self-healing properties to address the aforementioned issues encountered in brain surgery.

In this study, we synthesized LSPUs via one-shot polymerization, in which PCL diol, HPS, and IPDI were simultaneously added to the reactor. This method enabled more uniform distribution of dynamic disulfide bonds throughout the molecular chain structure of polyurethane, resulting in enhanced dynamic exchange of disulfide bonds and improved self-healing performance, as previously demonstrated in our work and that of other research teams.[24c,27] The structure of the polyurethane synthesized through this one-shot polymerization was depicted in **Figure 1**a, while Figure S1, Supporting Information, presented the synthesis scheme. The hard segment of the LSPUs was comprised of HPS and IPDI, while the soft segment was predominantly composed of PCL. The use of the one-shot polymerization technique might lead to the presence of a small proportion of urethane bonds in the soft segment. As previously stated, polyurethane is a block polymer composed of hard and soft segments, and the appropriate mechanical properties can be achieved by adjusting the ratio of hard to soft segments. Thus, in order to match the mechanical property of the dura mater, three types of LSPUs were synthesized using this method. Table S1, Supporting Information, provides a summary of the detailed basic data for each component, as well as the content of soft and hard segments. The ^{1}H-NMR (Figure 1b) spectrum confirmed the chemical structures of LSPUs, indicating that the desired polyurethane was successfully synthesized in accordance with the structural design. As shown in the table inset of Figure 1b, the proportions of each component in LSPUs derived from the ^{1}H-NMR integral value were nearly identical to their theoretical counterparts. In addition, we conducted ^{13}C-NMR and ^{1}H-NMR analyses of all the components, including polyurethanes and the reagents used in polyurethane synthesis, to double-check the synthesized structure, as illustrated in Figures S2 and S3, Supporting Information; the characteristic peaks of each component in LSPUs could be successfully assigned. In the FT-IR spectrum (Figure 1c), the N=C=O stretching vibration band at 2230 cm^{-1} disappeared, indicating that the -NCO group was completely reacted. The stretching vibration band at 1720 cm^{-1} belonged to the carbonyl group in the urethane bond of the hard segment and the ester bond of the PCL diol soft segment, whereas the stretching vibration band at 3350 cm^{-1} belonged to the -NH group in the urethane bond, indicating that the PCL diol was successfully introduced into the main chain of LSPUs. In addition, the characteristic chemical stretching vibration of the carbonyl group (1620–1800 cm^{-1}) was curve fitted and resolved into two spectral components using the Peakfit software (Figure 1d). The blue-filled curve was assigned to the H-bonding carbonyl groups of the hard segment, which represented the associated hard segments, or the formed hard phase. In addition, the red-filled one corresponded to the free the carbonyl groups of the hard segment dispersed in the soft phase as well as the PCL carbonyl groups of the soft phase. The degree of microphase separation (DPS) was calculated by the following Equation:[18a,23]

$$\mathrm{DPS} = A_{\mathrm{H}}/(A_{\mathrm{H}} + A_{\mathrm{F}}) \times 100\% \quad (1)$$

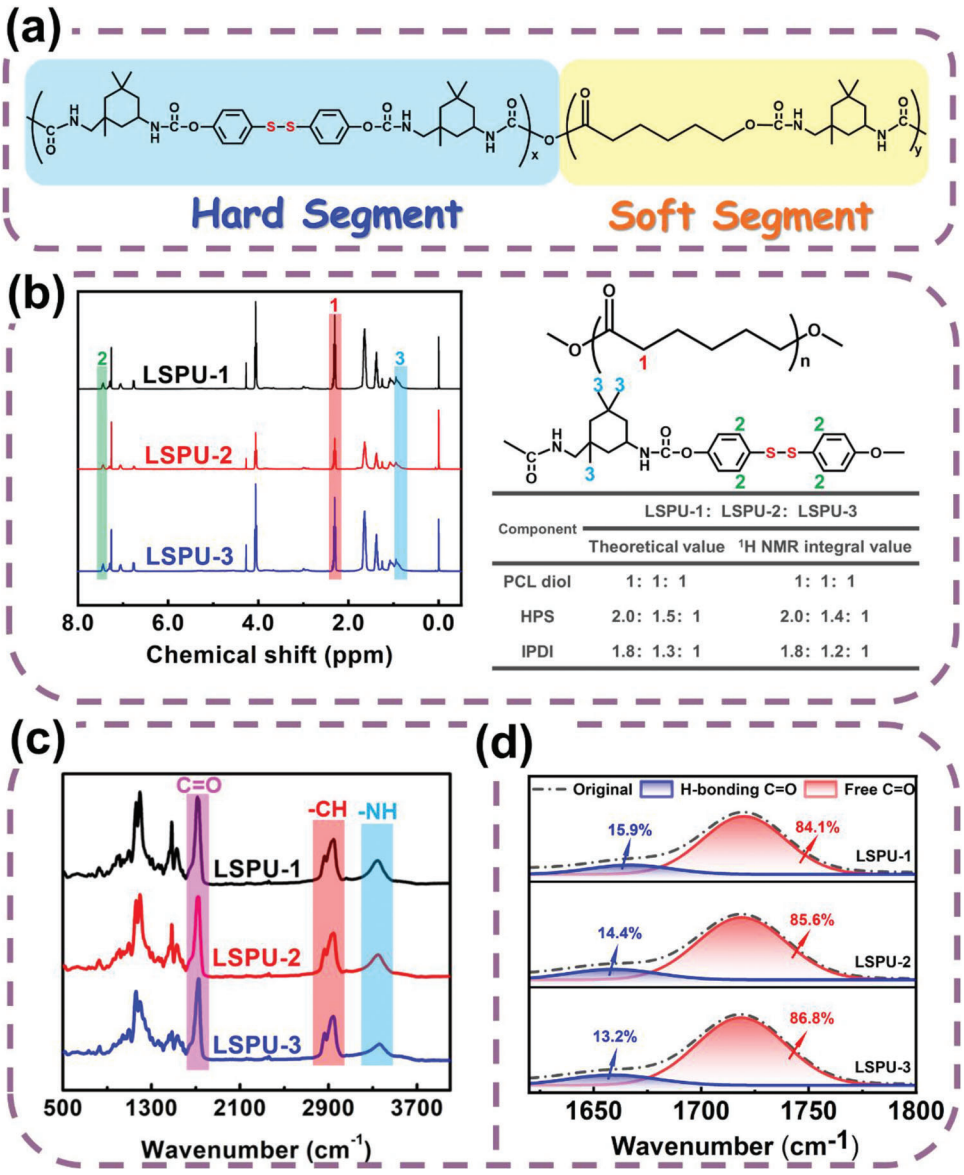

Figure 1. a) Chemical structure of the LSPUs; b) ^{1}H-NMR spectra of the LSPUs (LSPU-1–3); attribution of characteristic peaks of each component unit (top right) [the theoretical and ^{1}H-NMR integral values of each component were listed in the inset table (bottom right)]; c) FT-IR spectra of the LSPUs (LSPU-1–3); d) FT-IR absorbance spectra of the C=O stretching vibration (black dotted line): H-bonding C=O (blue filled area) and free C=O (red filled area) stretching vibration, respectively.

where, A_H and A_F represented the infrared absorption intensity of the blue and red blue filled curves, respectively. The calculated DPS values of LSPU-1–3 were 15.9%, 14.4%, and 13.2%, respectively. Thus, the high degree of microphase separation may aid in enhancing the tensile strength of the materials, as well as their deformation recovery capability. In addition, the higher degree of microphase separation resulted in a greater degree of crystallization, which aided in enhancing the barrier performance.

The molecular weight and molecular weight distribution index (PDI) of LSPUs were determined through gel permeation chromatography (GPC). It was evident from Figure S4, Supporting Information, that the molecular weight distribution of LSPUs was relatively concentrated, as the GPC curve of LSPUs displayed a single, large peak. The applied synthesis method made it possible to obtain a mass-average molar weight (M_w) greater than 69 000; the detailed molecular weight and PDI values of LSPUs are summarized in Table S1, Supporting Information. According to Figure S5, Supporting Information, S, C, N, and O elements were distributed uniformly across the surface of the LSPU-2. In addition, the specific contents of the above four elements in LSPUs increased or decreased regularly with the change of the soft/hard segment ratios, indicating that each component could be effectively regulated using the strategy employed in the current study (Table S2, Supporting Information). As shown in Figure S6, Supporting Information, each LSPU sample exhibited a single T_g, and the T_g increased linearly from −38.2 to −15.8 °C

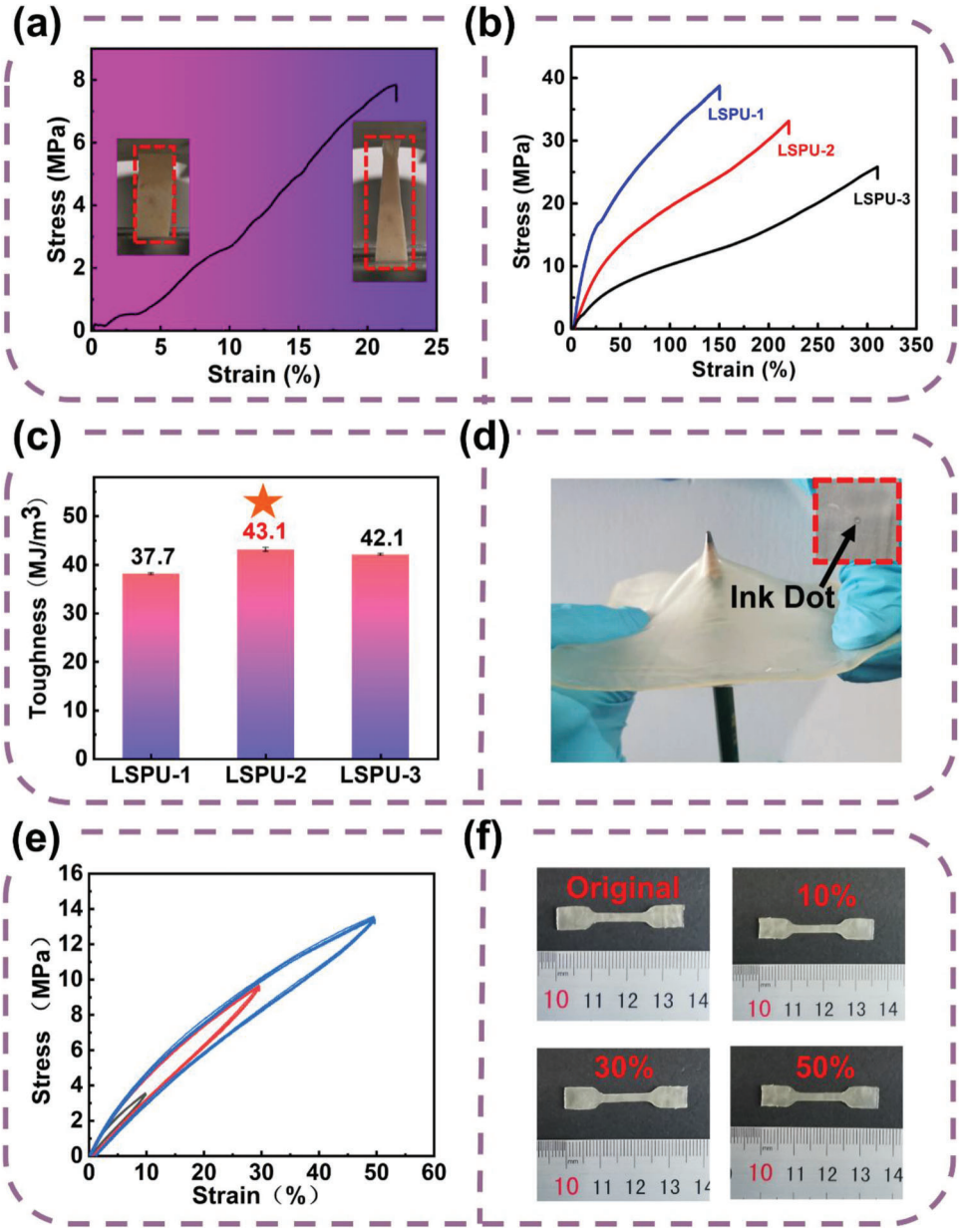

Figure 2. Typical stress–strain curve of a) the dura mater and b) the LSPUs (LSPU-1–3); c) Comparison chart of the fracture toughness of LSPUs (LSPU-1–3), and the red five-pointed star indicated the highest toughness; d) Demonstration of LSPU-2 puncture using a pen; the inset image was the intact film after puncture (top right); e) Sequential cyclic tensile curves of LSPU-2 at 10%, 30%, and 50% deformation for five times; f) Images of the standard LSPU-2 specimens after five cycles of stretching, representing the shape deformation. Note: the dura mater sample was obtained from a patient who underwent craniocerebral surgery at the Affiliated Lihuili Hospital of Ningbo University (protocol number KY2022PJ110).

as the hard segment content increased, demonstrating the gradual decrease in polymer chain mobility. The thermal gravimetric analyzer (TGA) curves demonstrated that LSPUs possessed excellent thermal stability (Figure S7, Supporting Information), and weight loss occurred at temperatures above 215.3 °C. The 5% weight loss temperature ($T_{5\%}$) ranged between 272.4 and 290.5 °C, allowing for the daily use of the artificial dura mater.

As an artificial dura mater, the mechanical properties of LSPUs are crucial because they must match the mechanical properties of the dura mater without exception. Comparing their mechanical properties was thus performed. According to **Figure 2**a, the tensile strain, modulus, and fracture toughness of the dura mater were 22%, 19.9 MPa, and 0.78 MJ m^{-3}, respectively. Its actual appearance and stretching process are depicted in detail in Movie S1, Supporting Information. The hard segment structure of the polyurethane is responsible for the material's strength and toughness, while the soft segment structure is responsible for the material's stretchability. Thus, the two are synergistically responsible for the resilience of the overall material. Accordingly, the mechanical property can be controlled by adjusting the ratio

of soft to hard segments. This strategy was used to synthesize LSPUs, and their mechanical properties are displayed in Figure 2b. The tensile strength decreased as the soft segment content increased, while the tensile strain increased naturally. LSPU-2 demonstrated the most remarkable mechanical property, with a tensile modulus of 22.4 MPa, which was comparable to that of dura mater. In addition, its tensile strain reached 220%, which was sufficient to meet the demands of the dura mater. All LSPUs exhibited adequate toughness to meet the requirements of brain surgery; additionally, LSPU-2 exhibited the highest fracture toughness of 43.1 MJ m^{-3} (Figure 2c), as summarized in Table S3, Supporting Information. In addition, puncture resistance was one of the essential properties that artificial dura mater must possess to prevent accidental damage. For the puncture resistance test, a pencil, the most prevalent sharp object in daily life, was chosen (Figure 2d). The outcomes demonstrated that LSPU-2 could effectively resist puncture without breaking. After the puncture test, the polyurethane film was able to return to its original condition due to its superior elasticity and toughness (Figure 2d, inset). In addition, LSPU-2 was subjected to a sequential cyclic tensile test five times under 10%, 30%, and 50% strain (Figure 2e), with the test details visible in Movie S2, Supporting Information. As evident, the specimen was able to return to its original state without experiencing any stress relaxation, demonstrating its remarkable ant fatigue property. Following the cyclic tensile tests, the specimen in Figure 2f changed minimally compared to the original specimen. The findings, therefore, demonstrate that LSPU-2 best matched the mechanical properties of the dura mater and possessed excellent puncture resistance, thereby protecting the brain effectively from accidental injury.

In addition to superior mechanical properties, the importance of biocompatibility for artificial dura mater is even more obvious. The neuronal cell is one of the most essential brain cells and also one of the most susceptible to death. Experiments on the cell viability of HT-22 neuronal cells demonstrated that LSPUs exhibited extremely low cytotoxicity. As depicted in **Figure 3**a,b, the control sample contained no polyurethane, whereas LSPU-0 lacked disulfide bonds. After 24 h of cell culture, bright-field images revealed that the morphology of HT-22 neuronal cells was well-preserved, and its specific structures, including axons and dendrites, were clearly visible with minimal cell death. The fluorescent live/dead staining images revealed a high percentage of surviving cells with no significant differences between the groups. The live cells cultured with LSPUs in Figure 3b were counted using Image J software, and all had cell viability rates greater than 99%. After 24 h of cell culture, the absorbance at 450 nm was also measured using the CCK-8 assay; it was proportional to the number of cells. The cell viability could be calculated by the following Equation (2):

$$\text{Cell viability} = \left[\left(A_s - A_b\right) / \left(A_c - A_b\right)\right] \times 100\% \quad (2)$$

where, A_s represented the absorbance of the determinant group (medium containing cells, CCK-8, and determinant), A_c represented the absorbance of a control group (medium containing cells and CCK-8, but no determinant), and A_b represented the absorbance of a blank group (medium containing CCK-8 and determinant, but no cells). Consequently, the percentage of viable cells in each group exceeded 99% (Figure 3c).

As depicted in Figure 3d, the absorbance at 450 nm of all groups significantly increased from day 1 to day 5, indicating that the cells in each group grew healthily and at a similar rate. Remarkably, it was discovered that the cell growth rate improved slightly with a decrease in the disulfide content of LSPUs, while HT-22 cells in each group maintained a high level of cell activity, indicating that disulfide bonds may have a slightly negative effect on neuronal cells. In addition, the on-skin tests were conducted to further examine the actual toxicity of LSPUs to humans. Four samples (LSPU-0, LSPU-1, LSPU-2, and LSPU-3) were attached to the skin of the volunteer for a week. During the 1-week observation period, there were no adverse skin reactions, such as erythema, pain, edema, or inflammation, as shown in Figure 3e. Experiments demonstrated that LSPUs are biocompatible and have the potential to be used as an artificial dura substitute.

The dura mater plays a crucial role in the prevention of cerebrospinal fluid leakage. As an artificial dura mater, the anti-leakage capability is essential. **Figure 4**a depicted the water permeability test that was conducted. All LSPUs exhibited better permeability coefficients than commercial polyurethane (CPU). As the hard segment content gradually decreased from LSPU-1 to LSPU-3, the permeability coefficient exhibited a weak downward trend, which may have been related to crystallinity. Consequently, differential scanning calorimeter (DSC) analysis was performed on LSPUs (Figure S8, Supporting Information), and it was discovered that the anti-leakage capacity of LSPUs was related to their crystallinity. Due to the reasonable soft/hard segment ratios of LSPUs, they were able to form a relatively ideal soft phase and hard phase, which was also essential for the formation of high crystallinity (Figure 1d). The crystallization produced a denser microstructure, thereby enhancing the permeability coefficient. Nevertheless, the phase separation of CPU was not as ideal as that of LSPUs, resulting in relatively poor crystallinity and a lower permeability coefficient. In contrast, the dura mater endures in the cerebrospinal fluid and never deforms. In this regard, LSPU-2 was selected for comparison with dura mater due to its superior overall performance, which includes modulus matching, toughness, biocompatibility, and permeability coefficient. LSPU-2 and the dura mater were simultaneously immersed in artificial cerebrospinal fluid every 10 days in order to measure the changes in mass and size. As depicted in Figure 4b, the mass of LSPU-2 and the dura mater remained nearly unchanged after 30 days of immersion, as did their shape. Additionally, we assembled a set of anti-leakage testing apparatuses in accordance with the industry-standard YY/T 0471.3-2004 and evaluated the anti-leakage performance of LSPU-2 (Figure 4c,d). The flat and clean diaphragm samples were sealed with nylon ties at the mouth of the polypropylene plastic tube containing artificial cerebrospinal fluid, and then the tube was inverted so that the artificial cerebrospinal fluid exerted 900 mm H_2O hydrostatic pressure on the diaphragm samples for 30 min. Consequently, no water leakage was observed on the filter paper, as depicted in Movie S3, Supporting Information, indicating that LSPU-2 had a good anti-leakage capacity and could satisfy the requirements of artificial dura mater.

The ability to self-heal is also required for artificial dura mater, as described previously. The dynamic disulfide bond was used as the driving force for self-healing due to its ability to perform dynamic bond exchange in order to achieve self-healing

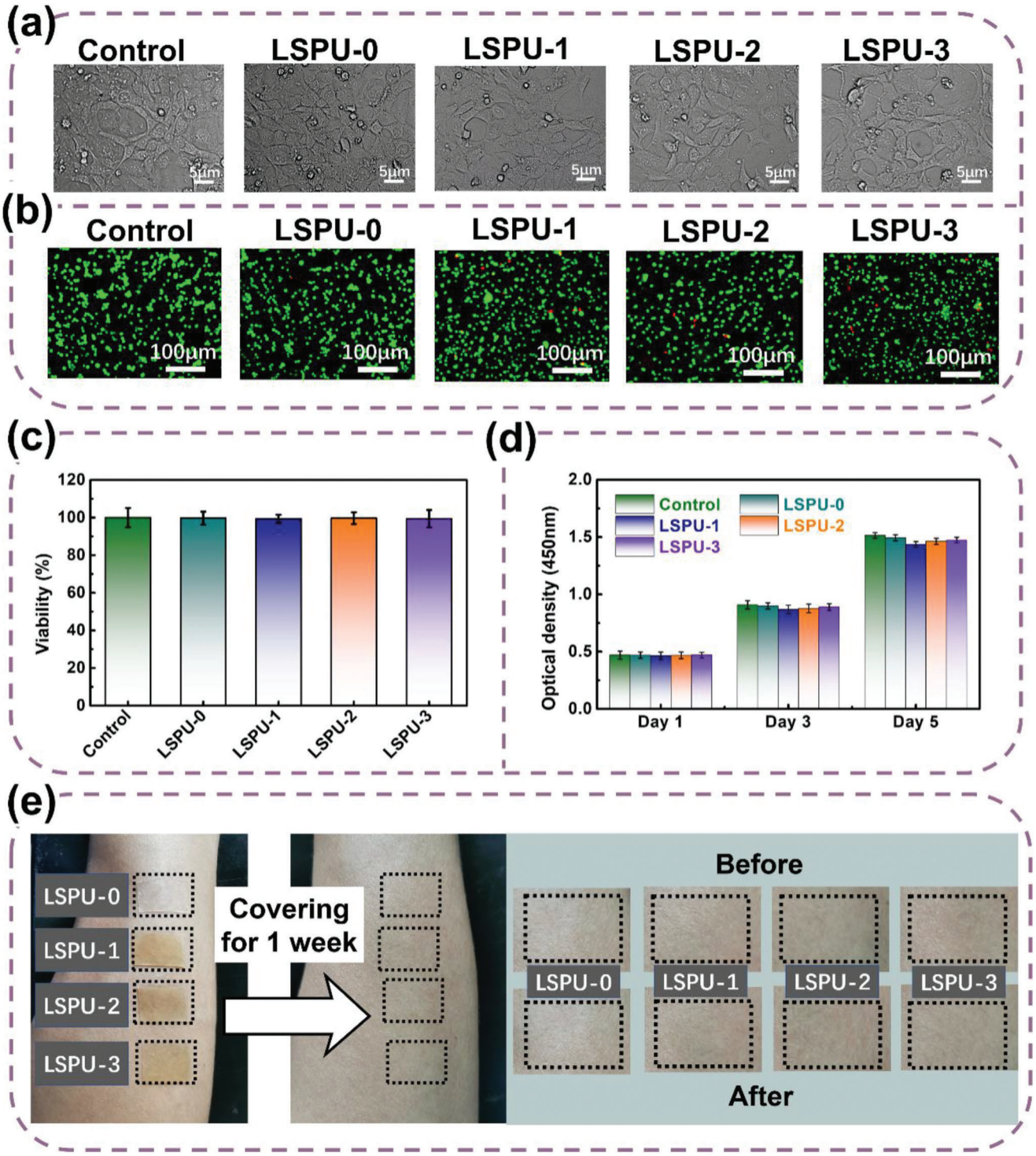

Figure 3. a) Bright-field images and b) fluorescent images of cells cultured in the incubation medium with the control samples, LSPU-0, LSPU-1, LSPU-2, and LSPU-3; c) Quantification of HT22 cell viability in different incubation groups; d) Absorption at 450 nm in CCK-8 assay of different incubation groups after 1, 3, and 5 days of incubation. The error bars show standard deviation; e) Images showing the skin irritation results of different samples on the forearms of the volunteer.

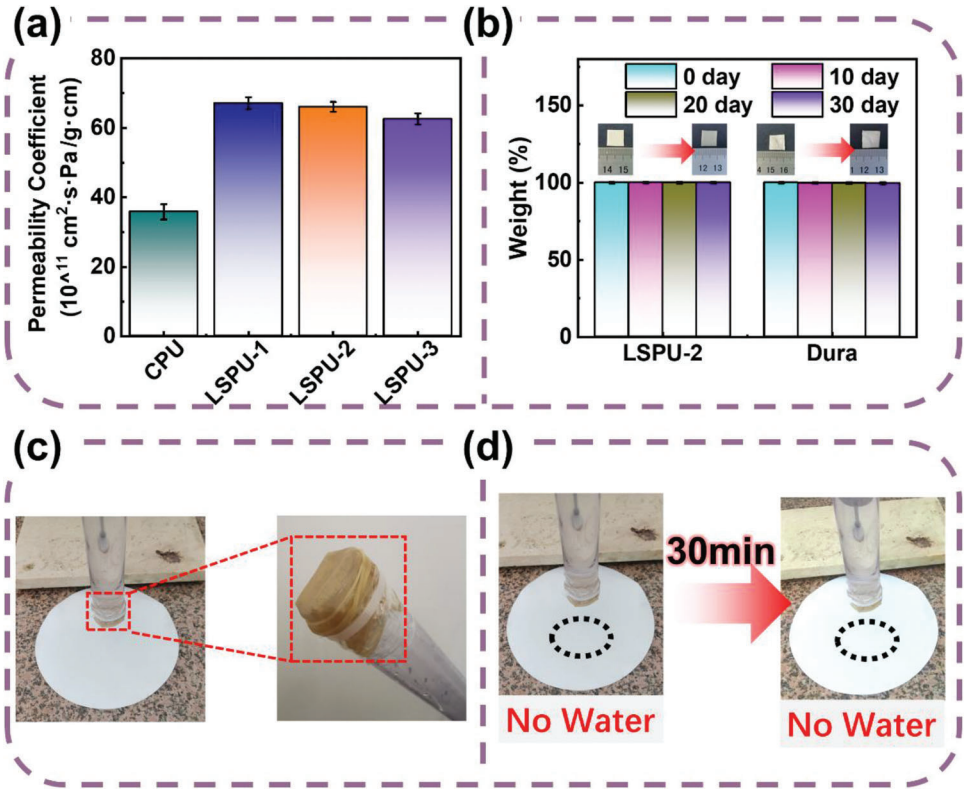

Figure 4. a) The permeability coefficient of CPU and LSPU-1–3; b) Weight changes in the LSPU-2 and the dura mater after soaking in artificial cerebrospinal fluid for 0–30 days; the inset images represent the samples before and after soaking; c) Enlarged view images of the sealing end in the anti-leakage test; d) Water leakage on filter paper before and after the leakage test.

performance at room temperature, as depicted in **Figure 5**a. Using the LSPU-2 as an example, Figure 5b displays the self-healing demonstration due to its optimal comprehensive properties, such as modulus matching with the dura mater, toughness, biocompatibility, and anti-leakage capacity. The scratches under the microscope gradually became blurrier as self-healing progressed, and the scratches vanished after 340 min, indicating complete self-healing. LSPU-2 self-healing tests were also conducted at 40.0, 50.0, and 60.0 °C, as depicted in Figure S9, Supporting Information. Laser confocal microscopy was used to examine the self-healing process intuitively and quantitatively. It is demonstrated that the entire process of self-healing began at the bottom and gradually progressed upward. As depicted in Figure 5c, the scratch depth decreased from 364 to 158 μm within 180 min and disappeared entirely after 340 min, confirming that LSPU-2 could self-heal completely at room temperature. As depicted in Movie S4, Supporting Information, the self-healing demonstration was also conducted. For a more accurate evaluation of the self-healing capability, the self-healing rate was calculated using the formula (3) presented in *Experimental Section* 4.6. Figure 5d summarized the self-healing speeds of LSPU-1–3 at various temperatures, and it was discovered that the self-healing speed increased as the temperature increased. The self-healing driving force and the mobility of the molecular chains had the greatest impact on the self-healing speeds of LSPUs.[16e,28] In this instance, the dynamic disulfide bond exchange is the self-healing driving force of LSPU. Concurrently, with the movement of the molecular chain, the dynamic disulfide bond was exchanged, resulting in the self-healing of polyurethane on a macroscopic scale. Molecular chain mobility could be analyzed from their glass transition temperature (T_g).[13b] As shown in Figure S6, Supporting Information, the T_gs of LSPUs were all below −0 °C, indicating that molecular chains could begin to move if the external temperature exceeded their T_g. With increasing temperature, the molecular chain moved more rapidly. Thus, with the acceleration of molecular chain mobility, the degree of dynamic disulfide bond exchange would be massively enhanced. Consequently, increasing the temperature could accelerate the rate of LSPU self-healing. However, LSPU-1 was incapable of complete self-healing below 50.0 °C due to its relatively less mobile molecular chain. In addition, it had the highest proportion of hard segments, which could associate to form the hard phase, limiting the mobility of the molecular chain and impeding the dynamic bond exchange.[13b] While the hard segment content of LSPU-2 was relatively lower, its molecular chain mobility was increased to the extent that room-temperature self-healing could be achieved at a rate of 1.18 μm min^{-1}. Thus, it had a faster self-healing rate at human body temperature (36.5 °C), which was beneficial for its use as an artificial dura mater. Creep experiments were performed on LSPUs by subjecting the samples to a constant tensile stress of 1 MPa at various temperatures. In Figures S10–S12, Supporting Information, the results demonstrated that the polyurethane molecular chains exhibited a certain degree of creep starting from room temperature, revealing their inherent mobility. This mobility further facili-

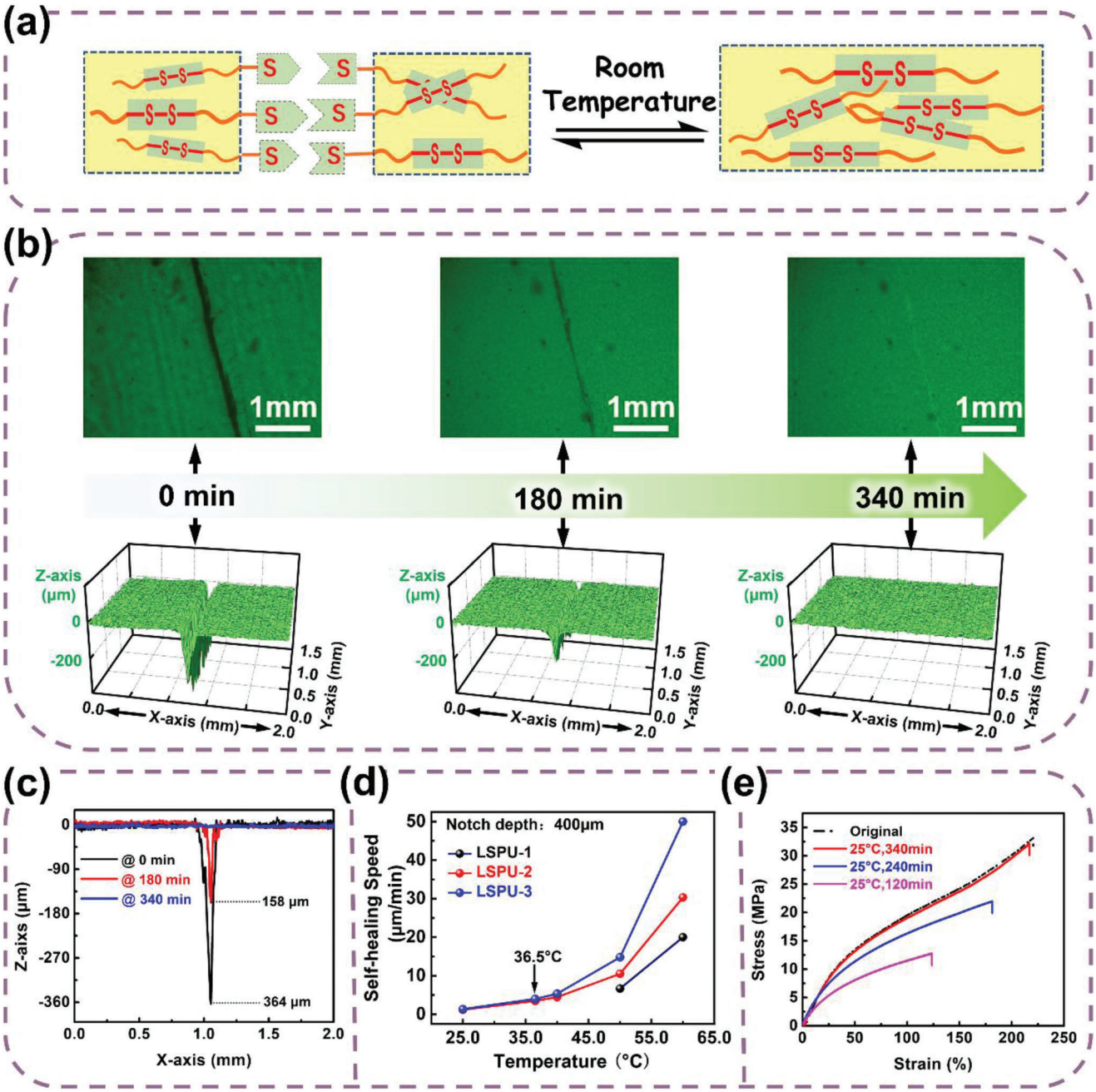

Figure 5. a) Self-healing mechanism of the LSPUs; dynamic disulfide bonds with the assistance of the appropriate molecular chain mobility; b) Optical microscope images of the self-healing process using a notched LSPU-2 film at room temperature; c) The 3D surface mapping microscope images of notched LSPU-2 during the self-healing process at room temperature; d) Temperature-dependent self-healing speed of the notched LSPU samples calculated from [notch size]/[self-healing period]; e) Stress–strain curves of the notched LSPU-2 self-healing at room temperature for different periods.

tated the exchange of disulfide bonds within the polyurethane molecular chains and consequently, enhanced the efficiency of self-healing. As the temperature increased, the degree of creep was found to proportionately increase, indicating that the molecular mobility of the polyurethane chains was amplified.[29] This phenomenon, in turn, accounted for the gradual acceleration of the self-healing speed with increasing temperature. Naturally, LSPU-3's self-healing performance was enhanced by the further reduction of hard segment content, at the expense of mechanical toughness. Therefore, the self-healing efficiency of LSPU-2 was subsequently evaluated semiquantitatively by testing its mechanical properties after self-healing for varying durations. The mechanical property of the standard specimen was restored by severing it in the middle and allowing it to heal on its own. As depicted in Figure 5e, the mechanical properties of LSPU-2 improved with time, and the toughness recovered to 38.5%,

66.3%, and 96.9% of the initial value after self-healing at room temperature for 120, 240, and 340 min, respectively. It is highly challenging to achieve both high stress and rapid self-healing ability for self-healing materials. Herein, we compared the stress and self-healing time of LSPU-2 with those of other recently reported materials capable of self-healing at room temperature. As illustrated in Figure S13, Supporting Information, LSPU-2 demonstrates notable advantages in both stress and self-healing time, achieving effective integration of high stress and rapid self-healing. Moreover, the mechanical properties of LSPU-2 are commensurate with those of human dura mater, and its self-healing and leak-proof properties satisfy completely the performance criteria demanded for artificial dura mater. Thus, such self-healing polyurethanes hold great promise for applications in the realm of artificial dura mater, which are unattainable by other self-healing materials.

3. Conclusion

In conclusion, we have designed and synthesized a series of polyurethanes to meet the practical requirements of artificial dura mater. LSPU-2 exhibited the best and most balanced comprehensive properties, including mechanical properties, biocompatibility, anti-leakage, and self-healing property. In terms of mechanical properties, its tensile modulus was identical to that of the dura mater, and its fracture toughness of 43.1 MJ m^{-3} resulted in exceptional puncture resistance. Cyclic tensile tests confirmed that LSPU-2 possessed exceptional ant fatigue properties and could withstand extended use. Regarding biocompatibility, bright-field images and fluorescent live/dead staining images demonstrated that mouse hippocampal neuron cells grew well after 24 h of culture, with a survival rate of over 99% and continuous reproduction. In addition, no negative lesions were observed in the human body as a result of the on-skin tests of the volunteer. In terms of anti-leakage capacity, the excellent permeability coefficient of LSPU-2 indicated its good barrier property to water vapor, as no leakage occurs even when subjected to 900 mm H_2O hydrostatic pressure. LSPU-2 also exhibited rapid self-healing performance at room temperature, with a rate of 1.18 μm min^{-1}, which accelerated with increasing temperature. Importantly, the rate of self-healing at human body temperature (36.5 °C) was increased to 3.48 μm min^{-1}, which was advantageous for use as an artificial dura mater. And the toughness after complete self-healing could be restored to 96.9% of the initial level (original: 33.1 MPa, self-healed: 32.1 MPa). In conclusion, LSPU-2 satisfies the requirements of artificial dura mater and is amenable to scalability; therefore, we anticipate that this study will facilitate the development of artificial dura mater. We will also continue to advance its practical application to real brain surgery.

4. Experimental Section

Materials: Polycaprolactone diols (PCL diol, Mn = 2000 g mol^{-1}) were produced by Maclean Biochemical Technology Co., Ltd. Dibutyltin dilaurate (DBTDL, 95%), bis(4-hydroxyphenyl) disulfide (HPS, 98%), isophorone diisocyanate (IPDI, 99%), anhydrous tetrahydrofuran (THF, 99.5%), 1,1,2,2-tetrachloroethane (TCE, 99.5%) and 1,4-bis(2-hydroxyethoxy)benzene (HQEE, 95%) were purchased from Aladdin (China) without further purification. The deionized water used in all the experiments was purified by water purification equipment (Molecular, MU-10L). Dulbeccos modified eagle medium (DMEM, Gibco), fetal bovine serum (FBS, Gibco), phosphate balanced solution (PBS, Corning), ethylene diamine tetraacetic acid (0.25% EDTA, Gibco), cell counting kit-8 (CCK-8, WST, Japan), abbkine live and dead cell double staining kit (Abbkine, KTA1001) and artificial cerebrospinal solution (ACSF, sterile) were provided by Ningbo Jingxi Biotechnology Co., Ltd.. Mouse hippocampal neuronal cells (HT-22 Cells, Procell, CL-0595) were purchased from Procell Life Science & Technology Co., Ltd. The medical tape (3 M, 2477P) used to attach LSPU to the skin for toxicity testing was purchased from Ningbo Jingxi Biotechnology Co., LTD. The dura mater was obtained from a patient undergoing craniocerebral surgery at the Affiliated Lihuili Hospital of Ningbo University in April 2022. This patient underwent emergency clearance of intracerebral hematoma and decompressive craniectomy due to severe craniocerebral trauma. During the operation, the first author cut a 2 × 2 cm section of dura mater and stored it in formalin for future study. Before this operation, the patient's wife had signed a consent form that had been approved by the Ethics Committee of the Affiliated Lihuili Hospital of Ningbo University (protocol number KY2022PJ110).

Polyurethane Synthesis: The entire feeding procedure was conducted in a glove box containing 99.999% Ar to prevent water contamination. PCL diol, HPS, DBTDL, and THF were introduced into a dry three-neck reactor fitted with a stir bar. The reactor was then sealed with a rubber plug and sealing ring, removed from the glove box, and transferred to an oil bath heated to 65.0 °C while stirring. After dissolving all of the aforementioned raw materials, isophorone diisocyanate (IPDI) was added dropwise to the reactor at a stoichiometric ratio of [NCO]/[OH]. After 6 h of polymerization, the synthesized polyurethane was precipitated in excess deionized water, washed multiple times to remove excess solvent, and then dried in a vacuum oven at 60.0 °C for 24 h to constant weight. The wt% ratios of [PCL diol]/[HPS] were varied by 1/1 (LSPU-1), 1.5/1 (LSPU-2), and 2/1 (LSPU-3) in the present study. The following additional amounts were made to LSPU-1 for each component: The final yield of LSPI-1 was 96.2% from PCL diols (12.00 g, 0.006 mol), HPS (12.00 g, 0.048 mol), IPDI (12.60 g, 0.057 mol), DBTDL (0.37 g, 0.586 mmol), THF (37.00 g). The following additional amounts were made to LSPU-2 for each component: The final yield of LSPI-2 from PCL diols (12.00 g, 0.006 mol), HPS (8.00 g, 0.032 mol), IPDI (8.86 g, 0.040 mol), DBTDL (0.30 g, 0.475 mmol), THF (29.00 g) was 95.8%. For LSPU-3, the following amounts of each component were added: PCL diols (12.00 g, 0.006 mol), HPS (6.00 g, 0.024 mol), IPDI (7.00 g, 0.031 mol), DBTDL (0.25 g, 0.396 mmol), THF (25.00 g); the yield of LSPI-3 was 96.5%. The chemical reaction formula was shown in Figure S1, Supporting Information. The synthesis method of LSPU-0 was the same as above, except that the HPS was replaced by HQEE. Figures S14–S16, Supporting Information, depict the chemical reaction formula, the ^{1}H NMR spectrum, and the ^{13}C NMR.

Pretreatment of Polyurethane: Several 4 × 5 mm rectangular flakes of polyurethane were cut and soaked in 75% alcohol for 2 h, followed by ultrasonication and UV irradiation for 1 h. This process was repeated three times and then immersed in deionized water for 24 h. Subsequently, the materials were placed in a 15 mL centrifuge tube, and 6 mL of DMEM (H) (with 1% double antibody) was added to the centrifuge tube, which was immersed in a cell culture incubator containing 5% CO_2 at 37.0 °C and replaced every 24 h for three times. Before use, 10% serum was added to the centrifuge tube and stored at 4.0 °C after the extract was filtered through a 0.22 μm filter for cell culture.

Cell Cytotoxicity Assay and Proliferation Assay: HT22 cells were plated in a 96-well plate, and PBS solution was added to the outermost ring of the 96-well plate prior to overnight incubation at 37.0 °C and 5% CO_2. The corresponding HT22 cells were then washed with an extracting solution for polyurethane that had been prepared in advance. On the first, third, and fifth days, the corresponding HT22 cells were incubated with the configured CCK8 solution for 4 h. Then, the corresponding absorbance values (OD) would be measured with a microplate reader equipped with a detection wavelength of 450 nm and a reference wavelength of 630 nm.

Cell Survival Assay: First, HT22 cells were seeded in 24-well plates and incubated overnight at 37.0 °C with 5% CO_2. The polyurethane materials that were previously prepared were then added to the corresponding HT22 cell wells. Subsequently, images of cells under a microscope at 100× magnification were captured. Moreover, additional images were captured after 24 h under identical conditions.

Cell Live/Dead Assay: Initially, HT22 cells were plated in 24-well plates and incubated overnight at 37.0 °C with 5% CO_2 in an incubator. Then, polyurethane materials that had been previously prepared were added to wells containing HT22 cells, and incubation was continued for 24 h. Following this, 0.5 mL of staining solution was added to the cells using the live and dead cell double staining kit. The cells were then incubated for 30 min at 37.0 °C in the dark and washed twice with PBS. Finally, viable cells were stained with the permeable green fluorescent LiveDye (E_x / E_m = 488 / 530 nm), whereas dead cells were stained with the impermeable red fluorescent NucleiDye (E_x / E_m = 535 / 617 nm). The cells were then imaged under the microscope at 40× magnification and the obtained images were merged for analysis.

Skin Irritation Test: The first author of this paper participated in this study as a volunteer, and 4 samples (LSPU-0, LSPU-1, LSPU-2, and LSPU-3) were attached to the forearm skin of the volunteer with adhesive. After 1 week, the four skin samples were extracted. Finally, the skin was photographed before and after the test to determine if any damage had occurred.

Stability Test in Artificial Cerebrospinal Fluid: The polyurethane film and dura mater, which were cut into 1 cm × 1 cm pieces and weighed, were immersed in artificial cerebrospinal fluid, dried every 10 days to evaluate the size and quality changes, and then their percentage changes were calculated.

The Anti-Leakage Test: In accordance with the industry standard YY/T 0471.3-2004 "Test Methods for Contact Wound Dressings Part III: Water Resistance," artificial cerebrospinal fluid was used to simulate the normal human brain intracranial pressure environment (80–180 mm H_2O) for the anti-leakage test of polyurethane film. The thickness of the sample film was similar to the actual thickness of human dura mater, which is about 300 µm.[30] Flat and clean diaphragm samples were sealed with nylon ties at the mouth of a polypropylene plastic tube containing artificial cerebrospinal fluid, and then the tube was inverted so that the artificial cerebrospinal fluid applied 900 mm H_2O hydrostatic pressure to the diaphragm samples for 30 min. Finally, water seepage was observed on the sample to evaluate its anti-leakage performance.

Characterization: The ^{1}H NMR and ^{13}C NMR were performed at room temperature on a Bruker AVANCE III (400 MHz) with tetramethylsilane (TMS) as the internal standard. PCL diol, IPDI, and LSPUs used trichloromethane as the solvent, and bis(4-hydroxyphenyl) disulfide used dimethyl sulfoxide as the solvent, and sample concentrations fell within a 1 – 5 wt% range. The FT-IR spectrum was measured using an Agilent Company Carry660+620 micro-infrared spectrometer with a scanning range of 500 to 4000 cm^{-1}. To determine the glass transition temperatures (T_gs) of the LSPUs, a differential scanning calorimeter (NETZSCH, Germany) was utilized to conduct the DSC test. The test was conducted in an atmosphere of 20 mL min^{-1} of nitrogen. To eliminate the thermal history, the sample was heated to 100.0 °C and held for 5 min, cooled to −100.0 °C and held for 5 min, and then heated to 100.0 °C once more. The rates of heating and cooling were both 10.0 °C min^{-1}. TGA (Mettler-Toledo TGA/DSC) experiment conducted in a dry N_2 atmosphere (50 mL min^{-1}) revealed thermal stability. ≈5–8 mg of the samples were heated to 800.0 °C with a heating rate of 20.0 °C min^{-1}. The mechanical properties and sequential cyclic tensile test of the polyurethanes were measured on a 1 kN universal testing machine (UTM, Zwick Instruments, Model: Z1.0). The test specimens were cut according to GB/T528-2009, with a thickness of 0.4 mm, length of 35 mm, a width of 2 mm, and a tensile speed of 50 mm min^{-1}. The self-healing capacity of polyurethane was observed in real-time with a polarizing microscope. The specific steps included cutting the polyurethane film into a rectangle, scratching the middle portion, and observing the self-healing process using a polarizing microscope with a hot stage (Olympus/BX 51TP, Instec H601, Japan). Simultaneously, the time required for complete self-healing at various temperatures was measured, and the self-healing rate was calculated using the following Equation (3):[26]

$$\text{Self-healing speed (mm/min)} = \text{notch size (mm)} / \text{self-healing period (min)} \quad (3)$$

Because the polyurethane film was completely cut during this self-healing test, the notch size was equivalent to the thickness of the polyurethane film, which was 0.4 mm. A laser confocal microscope (VK-X200K, Japan) was used to determine the 3D and scratch-depth healing process. In addition, the self-healing efficiency was derived from the mechanical recovery of the fractured splines. The distribution and percentage of each element on the substrate surface were tested using a scanning electron microscope (SEM, Thermo scientific Verios G4 UC, America) equipped with energy dispersive spectroscopy (EDS). The water vapor transmission rate (WTR) was determined in accordance with ASTM E96 using a water permeability tester (Labthink W3-060) at 90% RH and 38.0 °C, with the permeable surface area of the film fixed at 33 cm^2. The film's water permeability was determined by weighing the water that passed through it. Creep test were performed on a Q800 DMA (TA instruments, America). The samples were exposed to a constant stress of 1 MPa for 30 min at the test temperature (25.0, 36.5, 50.0, and 60.0 °C), after which the tension was removed and a 30-min recovery period was conducted. The strain of the sample was recorded throughout this process.

Supporting Information

Supporting Information is available from the Wiley Online Library or from the author.

Acknowledgements

This work was supported by National Natural Science Foundation of China (52003278 and 52211540393), the Project of Ningbo Leading Medical & Health Discipline (2022-F04), and S&T Innovation 2025 Major Special Program of Ningbo (2022Z139).

Conflict of Interest

The authors declare no conflict of interest.

Author Contributions

P.C. and F.L. contributed equally to this work.

Data Availability Statement

Research data are not shared.

Keywords

anti-leakage, biocompatibility, polyurethane, self-healing, the dura mater

Received: March 16, 2023
Revised: May 5, 2023
Published online: June 3, 2023

[1] a) A. Z. Wang, J. A. Bowman-Kirigin, R. Desai, L.-I. Kang, P. R. Patel, B. Patel, S. M. Khan, D. Bender, M. C. Marlin, J. Liu, J. W. Osbun, E. C. Leuthardt, M. R. Chicoine, R. G. Dacey, G. J. Zipfel, A. H. Kim, D. G. Denardo, A. A. Petti, G. P. Dunn, *Genome Med.* **2022**, *14*, 49; b) D. De Kegel, J. Vastmans, H. Fehervary, B. Depreitere, J. Vander Sloten, N. Famaey, *J. Mech. Behav. Biomed. Mater.* **2018**, *79*, 122.

[2] a) D. B. Macmanus, B. Pierrat, J. G. Murphy, M. D. Gilchrist, *Acta Biomater.* **2017**, *57*, 384; b) N. K. Mohtaram, J. Ko, A. Agbay, D. Rattray, P. O. Neill, A. Rajwani, R. Vasandani, H. L. Thu, M. B. G. Jun, S. M. Willerth, *J. Mater. Chem. B* **2015**, *3*, 7974; c) T. P. C. Van Doormaal, M. R. Germans, M. Sie, B. Brouwers, J. Fierstra, P. R. A. M. Depauw, P. A. Robe, L. Regli, *Neurosurgery* **2020**, *86*, E203.

[3] a) M. H. Khan, J. Rihn, G. Steele, R. Davis, W. F. Donaldson 3rd, J. D. Kang, J. Y. Lee, *SPINE* **2006**, *31*, 2609; b) V. Zelinkova, A. Brazinova, M. S. Taylor, M. Rusnak, D. Plancikova, J. Melichova, M. Majdan, *Brain Inj* **2019**, *33*, 830; c) C. A. Taylor, J. M. Bell, M. J. Breiding, L. Xu, *MMWR Surveill. Summ.* **2017**, *66*, 1.

[4] K. Rauen, L. Reichelt, P. Probst, B. Schäpers, F. Müller, K. Jahn, N. Plesnila, *Crit. Care Med.* **2020**, *48*, 1157.

[5] S. H. Halani, J. K. Chu, J. G. Malcolm, R. S. Rindler, J. W. Allen, J. A. Grossberg, G. Pradilla, F. U. Ahmad, *Neurosurgery* **2017**, *81*, 204.

[6] J. Henry, M. Amoo, A. Murphy, D. P. O'brien, *Acta Neurochir. (Wien)* **2021**, *163*, 1423.

[7] a) K. Nan, V. R. Feig, B. Ying, J. G. Howarth, Z. Kang, Y. Yang, G. Traverso, *Nat. Rev. Mater.* **2022**, *7*, 908; b) Z.-D. Zhang, L.-Y. Zhao, Y.-R. Liu, J.-Y. Zhang, S.-H. Xie, Y.-Q. Lin, Z.-N. Tang, H.-Y. Fang, Y. Yang, S.-Z. Li, J.-X. Liu, H.-S. Sheng, *Front. Surg.* **2022**, *9*, 877038; c) D. R. Walsh, A. M. Ross, S. Malijauskaite, B. D. Flanagan, D. T. Newport, K. D. Mcgourty, J. J. E. Mulvihill, *Acta Biomater.* **2018**, *80*, 237.

[8] a) Y. Hu, W. Dan, S. Xiong, Y. Kang, A. Dhinakar, J. Wu, Z. Gu, *Acta Biomater.* **2017**, *47*, 135; b) J. Ma, F. Wu, Z. Liu, Y. Fang, X. Chu, L. Zheng, A. Xue, K. Nan, J. Qu, L. Cheng, *Front. Med. (Lausanne)* **2022**, *9*, 888542; c) M. R. M. Jingwei Xie, W. Z. Ray, W. Liu, D. Y. Siewe, Y. Xia, *ACS Nano* **2010**, *4*, 5027.

[9] T. D. Mccall, D. W. Fults, R. H. Schmidt, *Surg. Neurol.* **2008**, *70*, 92.

[10] a) J. Liao, X. Li, W. He, Q. Guo, Y. Fan, *Acta Biomater.* **2021**, *130*, 248; b) J. Suwanprateeb, T. Luangwattanawilai, T. Theeranattapong, W. Suvannapruk, S. Chumnanvej, W. Hemstapat, *J. Mater. Sci. Mater. Med.* **2016**, *27*, 122.

[11] a) H. Sun, H. Wang, Y. Diao, Y. Tu, X. Li, W. Zhao, J. Ren, S. Zhang, *Brain Behav.* **2018**, *8*, 00907; b) D. Azzam, P. Romiyo, T. Nguyen, J. P. Sheppard, Y. Alkhalid, C. Lagman, G. N. Prashant, I. Yang, *World Neurosurg.* **2018**, *113*, 244; c) C. Chen, W. B. Ying, J. Li, Z. Kong, F. Li, H. Hu, Y. Tian, D. H. Kim, R. Zhang, J. Zhu, *Adv. Funct. Mater.* **2021**, *32*, 2106341.

[12] A. Alkhaibary, A. Alharbi, N. Alnefaie, A. Oqalaa Almubarak, A. Aloraidi, S. Khairy, *World Neurosurg.* **2020**, *139*, 445.

[13] a) R. Du, Z. Xu, C. Zhu, Y. Jiang, H. Yan, H.-C. Wu, O. Vardoulis, Y. Cai, X. Zhu, Z. Bao, Q. Zhang, X. Jia, *Adv. Funct. Mater.* **2019**, *30*, 1907139; b) C. Jiang, L. Zhang, Q. Yang, S. Huang, H. Shi, Q. Long, B. Qian, Z. Liu, Q. Guan, M. Liu, R. Yang, Q. Zhao, Z. You, X. Ye, *Nat. Commun.* **2021**, *12*, 4395.

[14] a) D. Y. Zhu, M. Z. Rong, M. Q. Zhang, *Prog. Polym. Sci.* **2015**, *49–50*, 175; b) M. W. Urban, *Prog. Polym. Sci.* **2009**, *34*, 679; c) J. F. Patrick, M. J. Robb, N. R. Sottos, J. S. Moore, S. R. White, *Nature* **2016**, *540*, 363.

[15] H. Tran, V. R. Feig, K. Liu, Y. Zheng, Z. Bao, *Macromolecules* **2019**, *52*, 3965.

[16] a) J. Chen, C. Li, H. Jia, Z. Shen, R. Zhao, T. Su, B. Xiang, X. Wang, D. W. Boukhvalov, Z. Luo, Y. Luo, *Macromolecules* **2022**, *55*, 4776; b) J. Chen, Y. Ma, T. Chen, Y. Du, J. Xu, D. Wang, J. Yang, P. Hu, J. Jing, B. Yao, J. Fu, *Adv. Funct. Mater.* **2023**, *33*, 2212564; c) F. Sun, L. Liu, T. Liu, X. Wang, Q. Qi, Z. Hang, K. Chen, J. Xu, J. Fu, *Nat. Commun.* **2023**, *14*, 130; d) J. Yang, D. Zhao, D. Yao, Y. Wang, H. Li, *Chem. Eng. J.* **2021**, *426*, 131595; e) J. Chen, Y. Gao, L. Shi, W. Yu, Z. Sun, Y. Zhou, S. Liu, H. Mao, D. Zhang, T. Lu, Q. Chen, D. Yu, S. Ding, *Nat. Commun.* **2022**, *13*, 4868.

[17] a) W. Cai, Z. Li, X. Mu, L. He, X. Zhou, W. Guo, L. Song, Y. Hu, *J. Hazard. Mater.* **2021**, *404*, 124106; b) L. He, X. Jiang, X. Zhou, Z. Li, F. Chu, X. Wang, W. Cai, L. Song, Y. Hu, *Appl. Surf. Sci.* **2022**, *581*, 152386.

[18] a) M. Wang, J. Hu, Y. Ou, X. He, Y. Wang, C. Zou, Y. Jiang, F. Luo, D. Lu, Z. Li, J. Li, H. Tan, *ACS Appl. Mater. Interfaces* **2022**, *14*, 17093; b) Y. Song, C. Sun, C. Tian, H. Ming, Y. Wang, W. Liu, N. He, X. He, M. Ding, J. Li, F. Luo, H. Tan, Q. Fu, *Chem. Sci.* **2022**, *13*, 5353; c) Z. Ma, Q. Huang, Q. Xu, Q. Zhuang, X. Zhao, Y. Yang, H. Qiu, Z. Yang, C. Wang, Y. Chai, Z. Zheng, *Nat. Mater.* **2021**, *20*, 859.

[19] a) H. Hu, J. Li, Y. Tian, S. Luo, J. Wang, W. B. Ying, F. Li, C. Chen, Y.-L. Zhao, R. Zhang, J. Zhu, *ACS Sustainable Chem. Eng.* **2021**, *9*, 13021; b) H. Hu, J. Li, Y. Tian, C. Chen, F. Li, W. B. Ying, R. Zhang, J. Zhu, *ACS Sustainable Chem. Eng.* **2021**, *9*, 3850.

[20] a) Q. Pearcy, M. Jeejo, M. Scholze, J. Tomlinson, J. Dressler, M. Zhang, J. Zwirner, *J. Mech. Behav. Biomed. Mater.* **2022**, *125*, 104866; b) R. Hemstapat, W. Suvannapruk, F. Thammarakcharoen, S. Chumnanvej, J. Suwanprateeb, *Proc Inst Mech Eng H* **2020**, *234*, 854.

[21] a) X. Guo, J. Liang, Z. Wang, J. Qin, Q. Zhang, S. Zhu, K. Zhang, H. Zhu, *Adv. Mater.* **2023**, *35*,2210092; b) R. Guo, Q. Zhang, Y. Wu, H. Chen, Y. Liu, J. Wang, X. Duan, Q. Chen, Z. Ge, Y. Zhang, *Adv. Mater.* **2023**, *35*, 2212130.

[22] a) Z. Kong, W. B. Ying, H. Hu, K. Wang, C. Chen, Y. Tian, F. Li, R. Zhang, *Polymer* **2020**, *210*, 123012; b) B. Ying, R. Z. Chen, R. Zuo, J. Li, X. Liu, *Adv. Funct. Mater.* **2021**, *31*, 2104665.

[23] W. B. Ying, H. Liu, P. Gao, Z. Kong, H. Hu, K. Wang, A. Shen, Z. Jin, L. Zheng, H. Guo, R. Zhang, J. Zhu, *Chem. Eng. J.* **2021**, *420*, 127691.

[24] a) L. He, Y. Zhu, F. Chu, W. Cai, L. Song, Y. Hu, *Appl. Surf. Sci.* **2022**, *602*, 154090; b) W. Cai, J. Wang, Y. Pan, W. Guo, X. Mu, X. Feng, B. Yuan, X. Wang, Y. Hu, *J. Hazard. Mater.* **2018**, *352*, 57; c) W. B. Ying, Z. Yu, D. H. Kim, K. J. Lee, H. Hu, Y. Liu, Z. Kong, K. Wang, J. Shang, R. Zhang, J. Zhu, R.-W. Li, *ACS Appl. Mater. Interfaces* **2020**, *12*, 11072.

[25] F. Fan, S. Ji, C. Sun, C. Liu, Y. Yu, Y. Fu, H. Xu, *Angew. Chem., Int. Ed. Engl.* **2018**, *57*, 16426.

[26] F. Li, Z. Xu, H. Hu, Z. Kong, C. Chen, Y. Tian, W. Zhang, W. Bin Ying, R. Zhang, J. Zhu, *Chem. Eng. J.* **2021**, *410*, 128363.

[27] I. Yilgör, E. Yilgör, G. L. Wilkes, *Polymer* **2015**, *58*, A1.

[28] V. Amoli, J. S. Kim, E. Jee, Y. S. Chung, S. Y. Kim, J. Koo, H. Choi, Y. Kim, D. H. Kim, *Nat. Commun.* **2019**, *10*, 4019.

[29] a) A. M. Grande, J. C. Bijleveld, S. J. Garcia, S. Van Der Zwaag, *Polymer* **2016**, *96*, 26; b) G. Zhang, T. Ngai, Y. Deng, C. Wang, *Macromol. Chem. Phys.* **2016**, *217*, 2172; c) X. Jian, Y. Hu, W. Zhou, L. Xiao, *Polym. Adv. Technol.* **2018**, *29*, 463.

[30] M. A. Reina, A. López-García, M. Dittmann, J. A. de Andrés, *Rev. Esp. Anestesiol. Reanim.* **1996**, *43*, 135.